



Probing nonlinear excitation conditions: photoluminescence and nonlinear absorption studies in laser-irradiated dielectrics

Peter S. Sneftrup¹ · Peter Juergens² · Vincenzo De Michele^{2,3} · José R. C. Andrade² · Marc J. J. Vrakking² · Peter Balling¹ · Alexandre Mermillod-Blondin²

Received: 7 November 2023 / Accepted: 17 January 2024 / Published online: 16 February 2024
© The Author(s) 2024

Abstract

Understanding the fundamentals of laser-matter interactions is crucial for developing and optimizing ultrafast laser processing strategies. In optically transparent solids, the key event by which energy is deposited in the material is through the generation of an electron–hole plasma via nonlinear excitation mechanisms. As the energy stored in the plasma relaxes, local distortions of the lattice may occur, such as point defects. These defects give rise to new discrete energy states located in the bandgap. In this study, we investigate how the presence of these energy states influences the transmission of ultrashort near-infrared laser pulses in fused silica. Experimental results of laser pulse transmission and photoluminescence from defects are correlated with optical microscopy of the irradiated spots, allowing us to identify different nonlinear interaction regimes. Numerical simulations indicate that photo-induced defects influence the nonlinear losses of ultrashort laser pulses and explain why a non-destructive damage regime with detectable excitation is only observed for a narrow intensity range in multipulse experiments.

Keywords Strong-field physics · Plasma formation · Nonlinear absorption · Ultrafast optics

1 Introduction

The investigation of nonresonant and nonlinear absorption phenomena in transparent dielectrics induced by high-intensity ultrashort laser pulses holds significant implications for various areas of research, ranging from fundamental studies to practical applications [1–3]. Furthermore, these interactions trigger subsequent processes that have notable importance in laser micromachining of transparent materials and in a multitude of cutting purposes [4–7]. The initial excitation of conduction-band electrons through strong-field excitation (SFE) [8] serves as a precursor for collisional excitation (CE), which is often considered the primary mechanism

responsible for achieving critical electron–hole plasma densities [1, 9–13], leading to permanent, non-destructive (Type I) modifications or even laser-induced damage or Type II modifications of the irradiated samples [14, 15].

Following the interaction with ultrashort laser pulses, the electron–hole plasma decays via multiple relaxation channels, resulting in the formation of self-trapped excitons and point defects, such as non-bridging oxygen hole centers (NBOHCs), which have been extensively studied in SiO₂ [16, 17]. Some defects further decay while emitting photons at specific wavelengths, enabling the tracking of their density and dynamics through distinct emission bands [16, 18–20].

The characterization of nonlinear losses, manifested as a loss of transmission (excluding plasma-induced reflection), has been widely employed to investigate laser-induced excitation in transparent solids [21–24]. After remaining constant in the linear interaction regime, a sudden decrease in transmission at higher intensities indicates that strong-field excitation (in combination with subsequent CE) produces a substantial concentration of free carriers. Previous studies have conducted nonlinear absorption measurements in various wide-bandgap materials, including SiO₂, Al₂O₃,

✉ Alexandre Mermillod-Blondin
mermillod@mbi-berlin.de

¹ Department of Physics and Astronomy, Aarhus University, Ny Munkegade 120, 8000 Aarhus C, Denmark

² Max-Born-Institute for Nonlinear Optics and Short Pulse Spectroscopy, Max-Born-Strasse 2A, 12489 Berlin, Germany

³ Laboratoire Hubert Curien UMR 5516, CNRS, IOGS, Université Jean Monnet Saint-Etienne, 42023 Saint-Etienne, France

and ZnSe [22, 25, 26]. Simplified rate-equation models have been employed to fit the nonlinear transmission drop, enabling the determination of the multiphoton order and corresponding coefficients [12, 22, 27, 28].

Experimental investigations in SiO₂ have revealed a memory effect imprinted on the nonlinear absorption measurements that is attributed to multiphoton excitation from pre-excited defect states and closely linked to dielectric breakdown [29]. Moreover, the impact of excitons on the nonlinear absorption, serving as readily excitable seed carriers, has been examined in a study by Grojo et al. [27]. It has been demonstrated that excitons cause a substantial decrease of the excitation threshold and the associated laser-induced damage threshold, reducing the required intensities for such effects to occur. Associated incubation effects that generally result in a monotonous decrease of the excitation threshold and correspondingly of the laser-induced damage threshold as a function of the applied number of pulses have been studied in various multipulse experiments [23, 30].

This study aims to establish correlations among multiple experimental observables, providing a comprehensive and generalized understanding of the distinct regimes of laser-driven nonlinearities in transparent solids. To achieve this, we combine transmission measurements with a characterization of the photoluminescence (PL) emitted from the laser-irradiated sample and post-mortem microscopic investigations. In the transmission measurements, we systematically increase and decrease the peak pulse intensity to examine changes in the material response resulting from laser-excitation processes (influenced by defect-seeded multiphoton excitation) while simultaneously using the PL signal as an indicator of the concentration of optically-active defects. Finally, the microscopic investigations are conducted to determine laser-induced damage, which we define as any change visible with the microscope. Supporting our experimental findings, a numerical model based on a single rate equation is utilized. Our results demonstrate that the emergence of a strong PL signal is a more sensitive probe for the onset of laser-induced damage in fused silica than the presence of a memory effect in the nonlinear absorption.

2 Experimental setup

In the experiment, a commercial Ytterbium-based laser source (Satsuma HP2 from Amplitude Laser) operated at 10 kHz and delivering 1030 nm laser pulses with a full-width at half-maximum duration of 280 fs was used. The laser beam was focused into the bulk of amorphous UV-grade fused silica samples (Corning 7980, thickness: 500 μm) with the help of a fused silica lens (focal length: 150 mm) giving a Gaussian beam waist in the absence of self-focusing of 88 μm. The intensity was controlled using a combination of

a zero-order half-wave plate and two thin-film polarizers. After interaction with the sample, the beam was collimated and directed onto an energy meter (Ophir PD10-C) to characterize the transmission through the laser-excited SiO₂ sample. We ensured that the collection angle of the power meter was sufficiently large to minimize the losses due to propagation effects (self-focusing, plasma defocusing, etc.). In addition, the plasma luminescence from the fused silica sample was analyzed with the help of a fiber spectrometer (Avantes AvaSpec-ULS2048XL-EVO).

Figure 1 shows the experimental setup (see Fig. 1a) together with exemplary results of the spectrally-resolved PL signal sampled at two different peak pulse intensities (see Fig. 1b) as well as the transmission of the near-infrared laser beam as a function of the peak pulse intensity (Fig. 1c). At a peak pulse intensity of 0.16 TW cm⁻² a spectrum centered around ~650 nm as expected for a PL spectrum associated with NBOHCs [31–34] is observed (see red line in Fig. 1b). At a higher peak pulse intensity of 0.19 TW cm⁻² the PL signal exhibits a ~ five-fold increase while at the same time another spectral component centered at ~550 nm becomes visible (green line in Fig. 1b). While the main peak at 650 nm originates from NBOHC emission [20, 34, 35], the secondary peak is attributed to plasma luminescence. In our data analysis, we will focus on the PL originating from the NBOHCs which is marked by the gray integration region from 630 to 700 nm. The measurements of the PL yield were supplemented with optical microscopy of the irradiated region (see insets in Fig. 2). These images were acquired

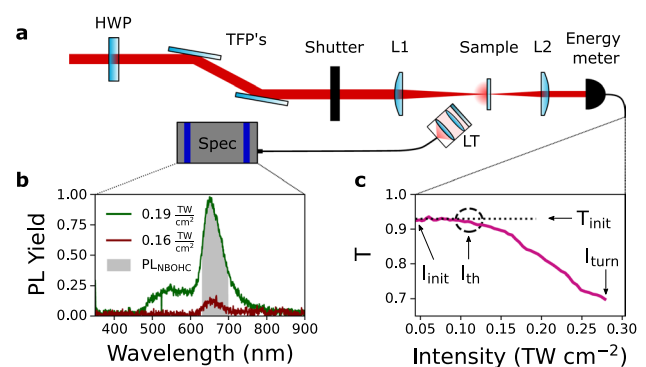


Fig. 1 Experimental setup and exemplary results for transmission and PL measurements in SiO₂. **a** Experimental setup. *HWP* Half-wave-plate, *TFP* thin-film polarizer, *L1* and *L2* lenses, *Spec* spectrometer, *LT* lens tube equipped with a shortpass filter to remove scattered pump light (Thorlabs FESH1000), one lens to collect the PL, and one to couple it into an optical fiber connected to the spectrometer. **b** PL spectra obtained at two different intensities (yield is shown in arbitrary units). The shaded gray area shows the region of integration used to obtain the PL originating from NBOHCs PL_{NBOHC} (630–700 nm). **c** Transmission of the laser pulses through a 500 μm thick fused silica sample as a function of peak pulse intensity up to a turning point intensity I_{turn}

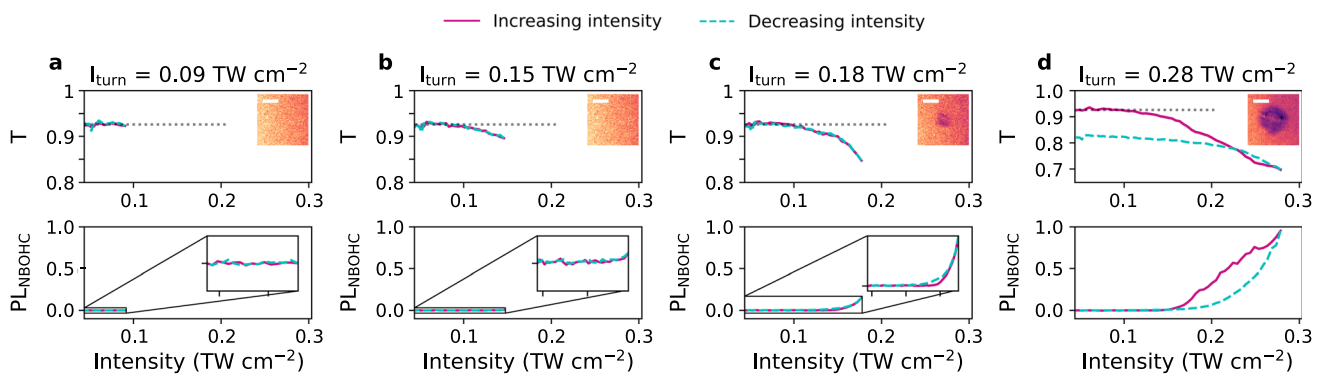


Fig. 2 Experimental results of the transmission T and of the integrated PL signal at four different values of I_{turn} . The solid magenta lines show data for increasing peak pulse intensity and the dashed cyan lines show data for decreasing peak pulse intensity while the dotted line marks the transmission due to Fresnel losses. In the transmission measurements, the insets show post-mortem microscope

images of the spots where the scalebar is $10\mu\text{m}$. Results obtained at a turn-around intensity **a** $I_{\text{turn}} = 0.09\text{ TW cm}^{-2}$. **b** $I_{\text{turn}} = 0.15\text{ TW cm}^{-2}$. **c** $I_{\text{turn}} = 0.18\text{ TW cm}^{-2}$. **d** $I_{\text{turn}} = 0.28\text{ TW cm}^{-2}$. Note that the transmission axis differs between panels and that the microscope image in **(a)** is the same as in **(b)** since no damage was visible at either of the two positions

in a plane transverse to the beam propagation direction with a back-illuminated microscope.

The transmission signal shown in Fig. 1c exhibits an initial transmission of ~ 0.93 (indicated by T_{init} in Fig. 1c) that is consistent with Fresnel-losses at the interfaces of the SiO_2 sample. After a constant, plateau-like region that is characteristic of the linear interaction regime, up to $\sim 0.11\text{ TW cm}^{-2}$, a drop of the transmission is found that is attributed to an apparent excitation threshold (labeled I_{th} in Fig. 1c) (determined by a drop of 1% in transmission).

To obtain the transmission curve shown in Fig. 1c we first move the sample so that the laser irradiates a pristine location, we set the peak pulse intensity $I_{\text{laser}} = I_{\text{init}}$, and we irradiate the sample for 1 s. As a next step, I_{laser} is incremented and the sample is again irradiated for 1 s. Note that the sample is not displaced between two exposures. This simple experimental sequence (intensity increase followed by exposure at a constant sample location) is repeated until $I_{\text{laser}} = I_{\text{turn}}$. Finally, we reproduce the whole sequence, but this time the intensity is gradually decreased down to I_{init} (not shown in Fig. 1c). To ensure statistical reliability, we maintain a constant number of shots at each intensity level (i.e. the $\sim 10,000$ laser pulses corresponding to a 1 s exposure), which means that the total number of pulses is dependent on I_{turn} . As a consequence, a steady-state of defect concentration and corresponding PL emission is attained at every intensity. Once I_{init} is reached, the sample is relocated to a fresh, pristine spot, and the entire procedure is repeated for a new value of I_{turn} . To assess the robustness of our findings, we conducted five repetitions of the measurement for every value of I_{turn} .

3 Experimental results and discussion

Experimental results at four different values of I_{turn} are shown in Fig. 2. Each panel represents a different excitation regime discernible through the employed experimental methodology. The measurements conducted at $I_{\text{turn}} = 0.09\text{ TW cm}^{-2}$, as depicted in Fig. 2a (upper panel), solely show a constant transmission as expected in the linear regime. As anticipated, no change in the material response is observed in the linear regime, resulting in an identical transmission when increasing and decreasing the intensity. Consistent with the fact that the excitation threshold within the sample is not surpassed and no electron-hole plasma is generated, no defect PL is detected (see lower panel of Fig. 2a). Correspondingly, no laser-induced damage is found using optical microscopy, as evidenced by the inset in the upper panel of Fig. 2(a).

In contrast, at $I_{\text{turn}} = 0.15\text{ TW cm}^{-2}$, a notable decline in transmission is observed for $I > 0.11\text{ TW cm}^{-2}$ (see Fig. 2b). After reaching I_{turn} and subsequently decreasing the peak pulse intensity to I_{init} , the transmission attains identical values as during the increase of the intensity. Still, no strong PL is observed (see lower panel of Fig. 2b), and no laser-induced damage is found in the post-mortem microscopy.

At $I_{\text{turn}} = 0.18\text{ TW cm}^{-2}$ the same behavior is observed in the transmission measurement only with a stronger loss of transmission at higher pulse intensities (see upper panel of Fig. 2c). In the PL measurement, however, a pronounced PL peak is now detected at 650 nm ($\sim 1.9\text{ eV}$) when the peak pulse intensity exceeds $\sim 0.15\text{ TW cm}^{-2}$.

The spectrally-integrated PL yield as a function of the near-infrared peak pulse intensity is shown in the lower panel of Fig. 2c and exhibits a nonlinear increase. With the help of optical microscopy, a damaged region (see upper panel of Fig. 2c) of ($\sim 10\mu\text{m}$ diameter) is observed in the irradiated area. The observed damage in the microscope image only causes a drop in transmission of the illuminating source of a few percent which is seemingly not detectable with direct transmission measurement using the pulsed laser source. The PL signal, on the other hand, evidently serves as a much more sensitive probe for the onset of laser-induced damage.

At the highest turn-around peak pulse intensity of 0.28 TW cm^{-2} (see Fig. 2d), the transmission drops to approximately 0.7. At the same time, a non-vanishing difference emerges between the transmission curves for increasing and decreasing peak pulse intensity. Notably, at intensities close to I_{init} , the transmission does not return to its initial value, indicating the presence of a permanent modification of the sample that affects its transmission even in the linear interaction regime (i.e. laser-induced damage as also supported by the microscope image in the inset of Fig. 2d). The loss of transmission is in part driven by strong scattering from the damaged region, causing less light to be collected by the collimating lens (L2 in Fig. 1a).

While in the case of $I_{\text{turn}} = 0.09\text{ TW cm}^{-2}$ the light-matter interaction is solely linear and no energy is transferred from the laser field to the sample, the excitation due to SFE and CE is sufficient to induce a significant energy absorption of the fundamental field at $I_{\text{turn}} = 0.15\text{ TW cm}^{-2}$. In fact, the observed loss of transmission can be fully attributed to absorption and not increased reflectivity or scattering as was ensured by the underdense plasma and a sufficiently large detector size. Note that at $I_{\text{turn}} = 0.15\text{ TW cm}^{-2}$ no PL or laser-induced damage is observed. The onset of transmission losses without the emission of a detectable PL signal (see Fig. 2b) can be interpreted as a marker of a non-destructive but ionizing interaction regime. The onset of the PL emission, together with the identification of laser-induced damage in the irradiated region by optical microscopy at a peak pulse intensity of 0.18 TW cm^{-2} , indicate a correlation between the evolution of the NBOHC signal and the appearance of a damaged region. Finally, the emergence of a difference between the two transmission curves at $I_{\text{turn}} = 0.28\text{ TW cm}^{-2}$ (as observed in Fig. 2d) can be partially attributed to a lowered excitation threshold due to the presence of photo-induced defects [29] and to scattering of the incoming laser radiation from the previously damaged region. In the present investigation, post-mortem microscopic investigations reveal unambiguous morphologies of laser-induced damage in all spots where I_{turn} is sufficient to generate a detectable NBOHC PL signal, even when no substantial difference between the forward and backward transmission

curves is observed. This confirms the conclusion drawn in Ref. [29] that the memory effect, leading to differences and a shift in the excitation threshold, is intimately associated with the onset of laser-induced breakdown. However, it appears that the onset of a PL signal attributed to photoinduced NBOHCs (see Fig. 2c) serves as a more sensitive probe for the initiation of laser-induced damage in bulk SiO_2 than the characterization of the nonlinear losses.

Thus, by using the three experimental methods (transmission, PL and post-mortem microscopic investigations), we can determine four different interaction regimes that are summarized in Fig. 2a–d. The linear interaction regime is characterized by a constant transmission, no detectable PL signal, and no visible damage (see Fig. 2a). The non-destructive interaction regime where nonlinear excitation mechanisms lead to the formation of an electron–hole plasma is characterized by a drop in transmission without the presence of a PL signal (see Fig. 2b). Furthermore, the analysis of Fig. 2c, d reveals the existence of two distinct regimes of permanent laser-induced damage. The first regime is characterized by a reversible alteration of the sample's transmission, indicating that the irradiation product is a pure phase object (i.e. a Type I modification, see Fig. 2c). In the second interaction mode (Type II modification, see Fig. 2d), the presence of laser-induced damage has dramatic consequences on the final transmission.

4 Numerical simulations

To further substantiate our interpretation and study the influence of photo-induced defects on the transmission, we performed numerical simulations based on a widely-used single rate equation for the population of the conduction band (see e.g. Refs. [10, 12, 25, 27, 36]). We emphasize that for a sufficient numerical treatment of the experimental conditions, a propagation model including self-focusing, plasma defocusing, and excitation such as the nonlinear Schrödinger equation [37] would be necessary. This, however, is beyond the scope of this paper. Instead, we gain insights into the influence of photo-induced defects from a simplified model by assuming a constant density of electrons through the depth of the sample. In the numerical model, the conduction-band-electron density dynamics $\rho(t)$ is estimated with the help of a single rate equation given by

$$\frac{\partial \rho(t)}{\partial t} = \Gamma_{\text{SFE}}(t) + \Gamma_{\text{CE}}(t) \quad (1)$$

where $\Gamma_{\text{SFE}}(t)$ denotes the SFE rate and $\Gamma_{\text{CE}}(t)$ the CE rate. Here we employ the Keldysh model [8] to estimate the SFE rate, while the carrier excitation dynamics resulting from CE are simulated using a modified Drude

model where the excitation probability is computed via $\Gamma_{CE}(t) = \sigma\rho(t)I(t)/E_{crit}$ with the absorption cross-section σ given by [38, 39]:

$$\sigma = \frac{k_0\omega_0\tau_c}{n_0^2\rho_{crit}(1 + \omega_0^2\tau_c^2)} \tag{2}$$

Here $k_0 = |\mathbf{k}|$ represents the magnitude of the wave vector and τ_c denotes the density-dependent electron–electron collision time [38]. Furthermore, the critical energy E_{crit} is defined via $E_{crit} = E_g[1 + (1/2\gamma^2)]$ with the adiabatic Keldysh parameter γ and ρ_{crit} corresponds to the critical electron density $\rho_{crit} = \epsilon_0 m^* \omega_0^2 / e^2$ with effective electron mass m^* , central laser frequency ω_0 and dielectric constant ϵ_0 .

Following the interaction of the intense ultrashort laser pulse with the SiO₂ sample, the population of the conduction band relaxes, leading to the possible formation and population of excitons or related intergap levels. Various models incorporating deep and shallow trap/defect levels exist in the literature [27, 40, 41]. However, the exact energy levels, relaxation probabilities from excited states into the distinct intergap states and the maximum population within these levels are essentially unknown. In our simulations we consider only one intergap level ($I_p^{DEF} = 4$ eV) meant to simulate NBOHCs. The initial population of the defect level ρ_{DEF} is chosen as the maximum conduction-band-electron density reached during the interaction of the laser pulse with the pristine material. To account for the limited number of states in the defect level, we limit ρ_{DEF} to 1×10^{18} cm⁻³. The density of electrons residing in the defect level at a time t is denoted as $\rho_{trap}(t)$. Thus, the modified rate equation, which takes into account the excitation from defect levels and the depopulation of the defect state, can be expressed as follows:

$$\frac{\partial\rho(t)}{\partial t} = \Gamma_{SFE}(t) + \Gamma_{CE}(t) + \Gamma_{SFE}^{trap}(t) \tag{3}$$

Here the photoexcitation rate from the defect level is determined by

$$\Gamma_{SFE}^{trap}(t) = \Gamma_0^{trap}(t) \left(1 - \frac{\rho_{trap}(t)}{\rho_{DEF}} \right), \tag{4}$$

with $\Gamma_0^{trap}(t)$ being the Keldysh photoexcitation rate for an ionization potential of I_p^{DEF} . An illustration of the numerical model is depicted in Fig. 3(i).

Numerical solutions of Eqs. 1 and 3 are shown in Fig. 3. We used the same laser parameters as in the experiment ($\tau = 280$ fs, $\lambda = 1030$ nm) and the material properties for fused silica (bandgap $E_g = 7.8$ eV, linear refractive index $n_0 = 1.45$ and reduced electron mass $m^* = 0.635 m_e$ [39, 42] with electron mass m_e). It should be noted that the intensities used in the simulation are much larger than those reported in the

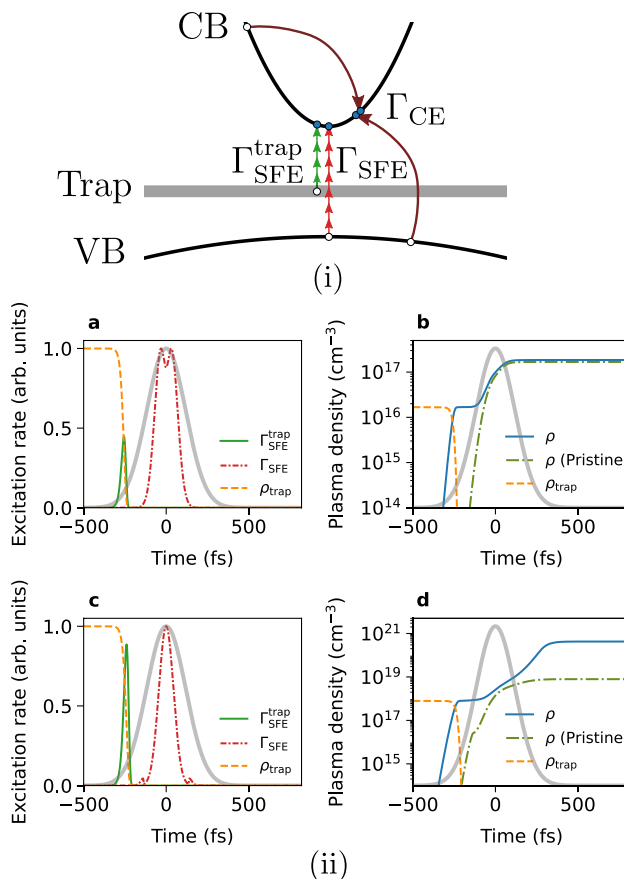


Fig. 3 (i): Illustration of the physical picture underlying the numerical model. Electrons can be excited through SFE either from the valence band (VB) to the conduction band (CB) or from the trap level (Trap) to the CB. Energetic CB electrons can undergo collisional excitation. (ii): Numerical simulations of the population transfer to the conduction band with and without the inclusion of excitation from an intergap defect level for a 1030 nm laser pulse with a pulse duration of 280 fs. **a, b** Peak intensity 6 TW cm⁻², **c, d** peak intensity 11.9 TW cm⁻². The thick gray line in all figures marks the intensity envelope on an arbitrary scale, and the orange line shows the density of electrons trapped in defect levels (ρ_{trap}) as a function of time. The solid blue lines in **(b)** and **(d)** show the conduction-band-electron density with the inclusion of defects, while the dashed green line is calculated for a pristine sample in the absence of defects

experimental results because these do not account for the significant increase in intensity due to self-focusing, as can also be observed directly by comparing the size of the laser damage seen in optical microscopy (see Fig. 2c, d) to the spot size of 88 μm. Numerical results obtained at a moderate peak intensity of 6 TW cm⁻² are shown in Fig. 3a, b. Figure 3a depicts the SFE rates $\Gamma_{SFE}(t)$ (red dash-dotted line) and $\Gamma_{SFE}^{DEF}(t)$ (green solid line) together with the normalized population of the defect state (yellow dashed line) and the temporal intensity envelope of the driving laser pulse (thick gray line). Notably, due to the much lower ionization potential, the defect-to-conduction band population transfer

occurs during the leading edge of the pulse and leads to a rapid depopulation of the defect level, hence providing seed carriers for subsequent processes at very early times during the interaction. The drop in the SFE rate at the peak of the pulse in Fig. 3a is due to the non-monotonous nature of the cycle-averaged Keldysh excitation rate as a function of the electric field amplitude. Figure 3b, d show the resulting dynamics of the conduction-band-electron density (see solid blue and dash-dotted green line) together with the population change in the defect level (see orange dashed line).

Despite the simplicity of the numerical model, which does not allow for a quantitative determination of the plasma formation and the associated nonlinear absorption, the qualitative trend clearly shows the influence of free carriers generated from defect intergap levels, as also concluded by Grojo et al. [27]. Due to the significantly smaller energy gap between the defect level and the conduction band edge compared to the bandgap, quasi-free carriers are available earlier during the pulse, facilitating CE to occur for longer times during the pulse, hence resulting in a higher total plasma density at the end of the pulse (see Fig. 3d).

To calculate the transmission through the sample based on the numerical simulations presented in Fig. 3, it is assumed that the loss of transmission is entirely dominated by linear absorption in the Drude plasma. The corresponding absorption coefficient, denoted as $\alpha(t)$, can be computed by the product of the conduction-band-electron density $\rho(t)$ and the absorption cross-section σ . Due to the long focal length of the focusing lens, which places us within a filamentary propagation regime [43], we make the assumption of uniform excitation as a function of the focusing depth across the sample. Applying the Beer–Lambert Law to determine absorption [44], denoted as $A(t)$, we employ the relationship $A(t) = 1 - \exp(-\alpha(t) \times \Delta z)$, where Δz represents the interaction length (for our simulations, we set $\Delta z = 500 \mu\text{m}$). Consequently, the absorption degree \mathcal{A} is determined by the equation $\mathcal{A} = \frac{\int A(t)I(t)dt}{\int I(t)dt}$, with $I(t)$ representing the intensity of the near-infrared driving pulse.

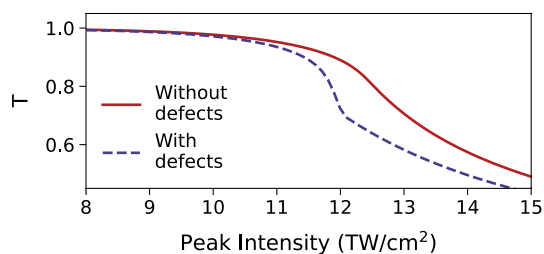


Fig. 4 Numerically calculated normalized transmission of a 1030 nm ultrashort laser pulse with a FWHM pulse duration of 280 fs in a pristine SiO_2 sample (red solid line) and in a pre-excited sample with a populated defect level (blue dashed line)

Numerical simulations depicting the transmission as a function of the peak intensity of a pulse with wavelength and pulse duration corresponding to those used in the experiment are presented in Fig. 4. The numerical results include a comparison between the transmission of the sample with photo-induced defects (blue dashed line) and the sample without defects (red solid line). In the simulation, no significant loss of transmission is observed up to peak intensities of approximately 10 TW cm^{-2} . However, at higher intensities, the transmission for the pristine sample shows a nonlinear decrease, reducing the transmission to ~ 0.5 at the highest peak intensity of 15 TW cm^{-2} . In the case of the pre-excited sample, where excitation of electrons from photo-induced defect states is possible, a much sharper drop in transmission is observed at a slightly lower threshold. These findings align with the results presented in Fig. 3(ii), demonstrating that even a small seed population generated through defect-to-conduction-band excitation triggers an efficient CE process (particularly evident in Fig. 3d). As a consequence, there is a rapid multiplication of the conduction-band-electron density, resulting in a sharp decline in transmission that saturates quickly as the entire laser pulse is depleted during propagation. The enhanced excitation for longer pulses in the presence of defects rapidly leads to laser-induced damage, thereby explaining why a regime of excitation without damage is only found for a narrow intensity range in the measurements presented in Fig. 2.

5 Conclusion

We have successfully presented an effective experimental approach to determine the interaction regimes between ultrashort laser pulses and fused silica. The key principle of our method involves systematic monitoring of the sample by progressively increasing and subsequently decreasing the peak pulse intensity and gradually reaching higher turning point intensities. By integrating measurements of the transmission, defect PL, and optical microscopy, we obtained independent indicators for plasma formation, defect formation, and laser-induced damage. Our findings indicate that the PL signal that we attribute to excited NBOHCs in fused silica serves as an excellent marker for laser-induced damage. In contrast, monitoring the transmission during the pulse intensity increase and decrease did not provide as intimate insights into the onset of laser-induced damage as the PL results. However, the onset of nonlinear absorption in the absence of a PL signal enables the identification of a non-destructive interaction regime where an electron–hole plasma is formed due to nonlinear excitation mechanisms. By gradually changing the turning point intensity, we were able to locate a narrow intensity window exhibiting clear nonlinear absorption without the presence of laser-induced

damage. Consistent with the findings by Grojo et al. [27], we propose that the observed change in transmission upon decreasing the pulse intensity after subjecting the sample to high-intensity laser pulses is attributed to the creation of intergap defect states, which act as initiators for the consecutive nonlinear excitation processes. Through numerical simulations based on a single-rate equation model, we demonstrate how the presence of pre-existing defects leads to the formation of a denser electron–hole plasma, resulting in reduced transmission and a shift of the excitation threshold to lower peak intensities. Our simulations highlight that the excitation of conduction-band electrons is governed primarily by a defect-seeded avalanche excitation mechanism, thereby creating a narrow nonlinear excitation regime in the absence of damage. Several novel experiments, such as high-harmonic generation from solids or photoconductive sampling require the onset of excitation without the presence of laser-induced damage. The presented method enables the determination of such a nonlinear interaction regime in intense light-matter experiments. It is worth noting that the formation of defects and subsequent PL emission is not exclusive to fused silica. Therefore, we anticipate that this method can be extended to other transparent dielectric materials displaying a pronounced PL response.

Acknowledgements P. B. acknowledges support by the Independent Research Foundation Denmark Natural sciences. A. M.-B. & P. J. acknowledge financial support from the Deutsche Forschungsgemeinschaft within CRC 1477 ‘Light-Matter Interactions at Interfaces’ (grant no. ID 441234705). A. M.-B. equally acknowledges the financial support from the Leibniz Association via grant No. K266/2019 (LAP-TON). V. d. M. acknowledges financial support from the Deutsche Forschungsgemeinschaft through the DFG/ANR grant INTRALAS (grant no. NA 1102/3-1).

Author Contributions PSS conceptualization, data acquisition, data analysis, writing. PJ conceptualization, writing, review and editing. VM methodology, review and editing. JRCA data acquisition, methodology, review and editing. MJJV review and editing, PB review and editing, funding acquisition. AMB conceptualization, review and editing, funding acquisition. All authors read and approved the manuscript.

Funding Open Access funding enabled and organized by Projekt DEAL.

Data availability The data generated and analysed during this study are available from the corresponding author upon reasonable request.

Declarations

Conflict of interest The authors have no competing interests to declare that are relevant to the content of this article. The authors declare that they have no known competing financial interests or personal relationships that could have appeared to influence the work reported in this paper.

Open Access This article is licensed under a Creative Commons Attribution 4.0 International License, which permits use, sharing, adaptation, distribution and reproduction in any medium or format, as long as you give appropriate credit to the original author(s) and the source,

provide a link to the Creative Commons licence, and indicate if changes were made. The images or other third party material in this article are included in the article’s Creative Commons licence, unless indicated otherwise in a credit line to the material. If material is not included in the article’s Creative Commons licence and your intended use is not permitted by statutory regulation or exceeds the permitted use, you will need to obtain permission directly from the copyright holder. To view a copy of this licence, visit <http://creativecommons.org/licenses/by/4.0/>.

References

1. B.C. Stuart et al., Nanosecond-to-femtosecond laser-induced breakdown in dielectrics. *Phys. Rev. B* **53**, 1749–1761 (1996). <https://doi.org/10.1103/PhysRevB.53.1749>
2. M. Malinauskas et al., Ultrafast laser processing of materials: from science to industry. *Light Sci. Appl.* **5**, e16133–e16133 (2016). <https://www.nature.com/articles/lsa2016133>
3. M. Garcia-Lechuga et al., Simultaneous time-space resolved reflectivity and interferometric measurements of dielectrics excited with femtosecond laser pulses. *Phys. Rev. B* **95**, 214114 (2017). <https://doi.org/10.1103/PhysRevB.95.214114>
4. R.R. Gattass, E. Mazur, Femtosecond laser micromachining in transparent materials. *Nat. Photonics* **2**, 219–225 (2008). <https://doi.org/10.1038/nphoton.2008.47>
5. F.J. Furch et al., Single-step fabrication of surface waveguides in fused silica with few-cycle laser pulses. *Opt. Lett.* **44**, 4267–4270 (2019). <https://opg.optica.org/ol/abstract.cfm?URI=ol-44-17-4267>
6. S. Nisar, L. Li, M.A. Sheikh, Laser glass cutting techniques—a review. *J. Laser Appl.* **25**, 042010 (2013). <https://doi.org/10.2351/1.4807895>
7. S.H. Chung, E. Mazur, Surgical applications of femtosecond lasers. *J. Biophotonics* **2**, 557–572 (2009). <https://doi.org/10.1002/jbio.200910053>
8. L.V. Keldysh, Ionization in the field of a strong electromagnetic wave. *Sov. Phys. JETP* **20**, 1307–1314 (1965)
9. D. Du, X. Liu, G. Korn, J. Squier, G. Mourou, Laser-induced breakdown by impact ionization in SiO₂ with pulse widths from 7 ns to 150 fs. *Appl. Phys. Lett.* **64**, 3071–3073 (1994). <https://doi.org/10.1063/1.111350>
10. A.-C. Tien, S. Backus, H. Kapteyn, M. Murnane, G. Mourou, Short-pulse laser damage in transparent materials as a function of pulse duration. *Phys. Rev. Lett.* **82**, 3883–3886 (1999). <https://doi.org/10.1103/PhysRevLett.82.3883>
11. P. Jürgens et al., Characterization of laser-induced ionization dynamics in solid dielectrics. *ACS Photonics* **9**, 233–240 (2022). <https://doi.org/10.1021/acsp Photonics.1c01417>
12. P.P. Rajeev, M. Gertszvolf, P.B. Corkum, D.M. Rayner, Field dependent avalanche ionization rates in dielectrics. *Phys. Rev. Lett.* **102**, 083001 (2009). <https://doi.org/10.1103/PhysRevLett.102.083001>
13. P. Balling, J. Schou, Femtosecond-laser ablation dynamics of dielectrics: basics and applications for thin films. *Rep. Prog. Phys.* **76**, 036502 (2013). <https://doi.org/10.1088/0034-4885/76/3/036502/meta>
14. K.M. Davis, K. Miura, N. Sugimoto, K. Hirao, Writing waveguides in glass with a femtosecond laser. *Opt. Lett.* **21**, 1729–1731 (1996). <https://opg.optica.org/ol/abstract.cfm?URI=ol-21-21-1729>
15. K. Mishchik et al., Ultrafast laser induced electronic and structural modifications in bulk fused silica. *J. Appl. Phys.* **114**, 133502 (2013). <https://doi.org/10.1063/1.4822313>
16. S. Guizard, P. Martin, G. Petite, P. D’Oliveira, P. Meynadier, Time-resolved study of laser-induced colour centres in. *J. Phys.*

- Condens. Matter **8**, 1281 (1996). <https://doi.org/10.1088/0953-8984/8/9/018>
17. C. Itoh, K. Tanimura, N. Itoh, Optical studies of self-trapped excitons in SiO₂. *J. Phys. C Solid State Phys.* **21**, 4693 (1988). <https://doi.org/10.1088/0022-3719/21/26/017/meta>
 18. G. Sigel, M. Marrone, Photoluminescence in as-drawn and irradiated silica optical fibers: an assessment of the role of non-bridging oxygen defect centers. *J. Non Cryst. Solids* **45**, 235–247 (1981). <https://www.sciencedirect.com/science/article/pii/S0022309381901903>
 19. A. Morana et al., Origin of the visible absorption in radiation-resistant optical fibers. *Opt. Mater. Express* **3**, 1769–1776 (2013). <https://opg.optica.org/ome/abstract.cfm?URI=ome-3-10-1769>
 20. V.D. Michele et al., Near-IR- and UV-femtosecond laser waveguide inscription in silica glasses. *Opt. Mater. Express* **9**, 4624–4633 (2019). <https://opg.optica.org/ome/abstract.cfm?URI=ome-9-12-4624>
 21. D.M. Rayner, A. Naumov, P.B. Corkum, Ultrashort pulse nonlinear optical absorption in transparent media. *Opt. Express* **13**, 3208–3217 (2005). <https://opg.optica.org/oe/abstract.cfm?URI=oe-13-9-3208>
 22. D. Grojo et al., Long-wavelength multiphoton ionization inside band-gap solids. *Phys. Rev. B* **88**, 195135 (2013). <https://doi.org/10.1103/PhysRevB.88.195135>
 23. Z. Guo et al., Energy deposition and incubation effects of nonlinear absorption of ultrashort laser pulses in dielectrics. *Opt. Express* **30**, 10317–10328 (2022). <https://opg.optica.org/oe/abstract.cfm?URI=oe-30-7-10317>
 24. E. Migal, E. Mareev, E. Smetanina, G. Duchateau, F. Potemkin, Role of wavelength in photocarrier absorption and plasma formation threshold under excitation of dielectrics by high-intensity laser field tunable from visible to mid-ir. *Sci. Rep.* **10**, 14007 (2020). <https://www.nature.com/articles/s41598-020-70862-w>
 25. F. Quéré, S. Guizard, P. Martin, Time-resolved study of laser-induced breakdown in dielectrics. *Europhys. Lett.* **56**, 138 (2001). <https://doi.org/10.1209/epl/i2001-00499-9>
 26. V.V. Temnov, K. Sokolowski-Tinten, P. Zhou, A. El-Khamhawy, D. Von Der Linde, Multiphoton ionization in dielectrics: comparison of circular and linear polarization. *Phys. Rev. Lett.* **97**, 237403 (2006). <https://doi.org/10.1103/PhysRevLett.97.237403>
 27. D. Grojo et al., Exciton-seeded multiphoton ionization in bulk SiO₂. *Phys. Rev. B* **81**, 212301 (2010). <https://doi.org/10.1103/PhysRevB.81.212301>
 28. A. Okhrimchuk, V. Mezentsev, H. Schmitz, M. Dubov, I. Benion, Cascaded nonlinear absorption of femtosecond laser pulses in dielectrics. *Laser Phys.* **19**, 1415–1422 (2009). <https://doi.org/10.1134/S1054660X09070081>
 29. P.P. Rajeev et al., Memory in nonlinear ionization of transparent solids. *Phys. Rev. Lett.* **97**, 253001 (2006). <https://doi.org/10.1103/PhysRevLett.97.253001>
 30. D. Ashkenasi, M. Lorenz, R. Stoian, A. Rosenfeld, Surface damage threshold and structuring of dielectrics using femtosecond laser pulses: the role of incubation. *Appl. Surf. Sci.* **150**, 101–106 (1999). <https://www.sciencedirect.com/science/article/pii/S0169433299002287>
 31. A. Beaudier, F.R. Wagner, J.-Y. Natoli, Using NBOHC fluorescence to predict multi-pulse laser-induced damage in fused silica. *Opt. Commun.* **402**, 535–539 (2017). <https://www.sciencedirect.com/science/article/pii/S0030401817305497>
 32. J. Qian et al., Tunable point defects in hydroxyl fused silica enabled by ultrashort laser pulses: photostimulated luminescence and functional module fabrication. *Opt. Mater. Express* **10**, 1241–1248 (2020). <https://opg.optica.org/ome/abstract.cfm?URI=ome-10-5-1241>
 33. V. De Michele et al., Photoluminescence of point defects in silicon dioxide by femtosecond laser exposure. *Phys. Status Solidi A* **218**, 2000802 (2021). <https://doi.org/10.1002/pssa.202000802>
 34. V. De Michele et al., Multiphoton process investigation in silica by uv femtosecond laser. *J. Non-Cryst. Solids* **580**, 121384 (2022). <https://www.sciencedirect.com/science/article/pii/S0022309321007456>
 35. L. Skuja, *Optical Properties of Defects in Silica* (Springer, Dordrecht, 2000), pp.73–116. https://doi.org/10.1007/978-94-010-0944-7_3
 36. B. Stuart, M. Feit, A. Rubenchik, B. Shore, M. Perry, Laser-induced damage in dielectrics with nanosecond to subpicosecond pulses. *Phys. Rev. Lett.* **74**, 2248 (1995). <https://doi.org/10.1103/PhysRevLett.74.2248>
 37. G. Fibich, *The Nonlinear Schrödinger Equation* (Springer, Cham, 2015). <https://doi.org/10.1007/978-3-319-12748-4>
 38. M. Jupé, L. Jensen, A. Melnikaitis, V. Sirutkaitis, D. Ristau, Calculations and experimental demonstration of multi-photon absorption governing fs laser-induced damage in titania. *Opt. Express* **17**, 12269–12278 (2009). <https://opg.optica.org/oe/abstract.cfm?URI=oe-17-15-12269>
 39. P. Jürgens, M.J.J. Vrakking, A. Husakou, R. Stoian, A. Mermillod-Blondin, Plasma formation and relaxation dynamics in fused silica driven by femtosecond short-wavelength infrared laser pulses. *Appl. Phys. Lett.* **115**, 191903 (2019). <https://doi.org/10.1063/1.5117837>
 40. S. Mao et al., Dynamics of femtosecond laser interactions with dielectrics. *Appl. Phys. A* **79**, 1695–1709 (2004). <https://doi.org/10.1007/s00339-004-2684-0>
 41. L.A. Emmert, M. Mero, W. Rudolph, Modeling the effect of native and laser-induced states on the dielectric breakdown of wide band gap optical materials by multiple subpicosecond laser pulses. *J. Appl. Phys.* **108**, 043523 (2010). <https://doi.org/10.1063/1.3457791>
 42. L. Sudrie et al., Femtosecond laser-induced damage and filamentary propagation in fused silica. *Phys. Rev. Lett.* **89**, 186601 (2002). <https://doi.org/10.1103/PhysRevLett.89.186601>
 43. N.T. Nguyen, A. Saliminia, W. Liu, S. L. Chin, R. Vallée, Optical breakdown versus filamentation in fused silica by use of femtosecond infrared laser pulses. *Opt. Lett.* **28**, 1591–1593 (2003). <https://opg.optica.org/ol/abstract.cfm?URI=ol-28-17-1591>
 44. P. Balling, Laser Coupling and Relaxation of the Absorbed Energy: Metals, Semiconductors, and Dielectrics, pp. 1–58 (2020). https://doi.org/10.1007/978-3-319-69537-2_10-1

Publisher's Note Springer Nature remains neutral with regard to jurisdictional claims in published maps and institutional affiliations.